ACSNANO
www.acsnano.org
ARTICLE

Surface-Enhanced Raman Scattering Active Gold Nanoparticles with Enzyme-Mimicking Activities for Measuring Glucose and Lactate in Living Tissues

Yihui Hu,[†] Hanjun Cheng,[†] Xiaozhi Zhao,[‡] Jiangjiexing Wu,[†] Faheem Muhammad,[†] Shichao Lin,[†] Jian He,[§] Liqi Zhou,[∥] Chengping Zhang,[⊥] Yu Deng,[⊥] Peng Wang,[∥] Zhengyang Zhou,*[,§] Shuming Nie,[†,#] and Hui Wei*[,†,¶]

[†]Department of Biomedical Engineering, College of Engineering and Applied Sciences, Collaborative Innovation Center of Chemistry for Life Sciences, Nanjing National Laboratory of Microstructures, Nanjing, Jiangsu 210093, China

[‡]Department of Urology and [§]Department of Radiology, Nanjing Drum Tower Hospital, the Affiliated Hospital of Nanjing University Medical School, Nanjing, Jiangsu 210008, China

[∥]Department of Materials Science and Engineering, College of Engineering and Applied Sciences, [⊥]Jiangsu Key Laboratory of Vehicle Emissions Control, Center of Modern Analysis, and [¶]State Key Laboratory of Analytical Chemistry for Life Science, School of Chemistry and Chemical Engineering, Nanjing University, Nanjing, Jiangsu 210093, China

[#]Department of Biomedical Engineering, Emory University, Atlanta, Georgia 30322, United States

Supporting Information

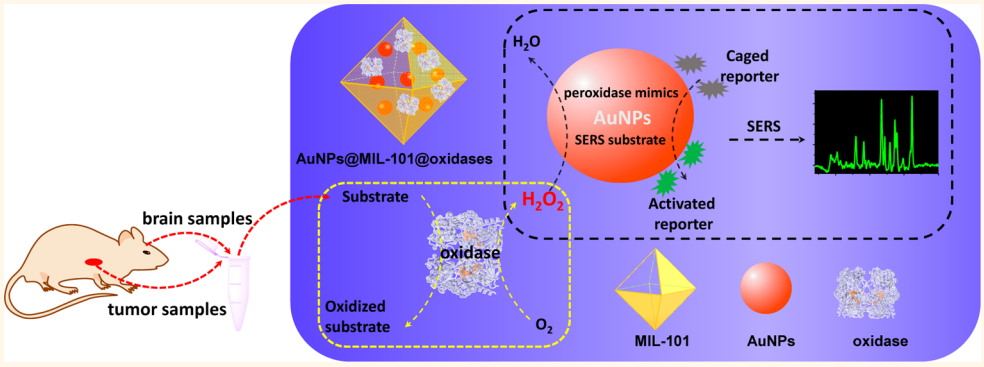

ABSTRACT: Gold nanoparticles (AuNPs) with simultaneous plasmonic and biocatalytic properties provide a promising approach to developing versatile bioassays. However, the combination of AuNPs' intrinsic enzyme-mimicking properties with their surface-enhanced Raman scattering (SERS) activities has yet to be explored. Here we designed a peroxidase-mimicking nanozyme by *in situ* growing AuNPs into a highly porous and thermally stable metal−organic framework called MIL-101. The obtained AuNPs@MIL-101 nanozymes acted as peroxidase mimics to oxidize Raman-inactive reporter leucomalachite green into the active malachite green (MG) with hydrogen peroxide and simultaneously as the SERS substrates to enhance the Raman signals of the as-produced MG. We then assembled glucose oxidase (GOx) and lactate oxidase (LOx) onto AuNPs@MIL-101 to form AuNPs@MIL-101@GOx and AuNPs@MIL-101@LOx integrative nanozymes for *in vitro* detection of glucose and lactate *via* SERS. Moreover, the integrative nanozymes were further explored for monitoring the change of glucose and lactate in living brains, which are associated with ischemic stroke. The integrative nanozymes were then used to evaluate the therapeutic efficacy of potential drugs (such as astaxanthin for alleviating cerebral ischemic injuries) in living rats. They were also employed to determine glucose and lactate metabolism in tumors. This study not only demonstrated the great promise of combining AuNPs' multiple functionalities for versatile bioassays but also provided an interesting approach to designing nanozymes for biomedical and catalytic applications.

KEYWORDS: *bioassays for living systems, enzyme mimics, glucose, gold nanoparticles, metal−organic framework, nanozymes, surface-enhanced Raman scattering*

Received: February 9, 2017
Accepted: May 26, 2017
Published: May 26, 2017

DOI: 10.1021/acsnano.7b00905
ACS Nano 2017, 11, 5558−5566

Gold nanoparticles (AuNPs) possess extraordinary surface-enhanced Raman scattering (SERS) activities and catalytic properties, which enable prospective applications in bionanomedicine and advanced catalysis.[1−10] Until now, AuNPs have been used to catalyze various important reactions, such as CO oxidation and C−C coupling reactions.[11,12] AuNPs are usually considered to be inert for biological catalysis. Unexpectedly, Rossi *et al.* found that citrate-coated AuNPs exhibited glucose oxidase (GOx)-mimicking activity for the catalytic oxidation of glucose with oxygen.[13] Such catalytic nanomaterials with enzyme-like activities are collectively called "nanozymes".[14−27] Since then, ever-growing interest has been devoted to mimicking natural enzymes with AuNPs.[28−35] For example, Gao *et al.* utilized AuNPs to mimic peroxidase for integrin detection.[36] Yin and co-workers recently demonstrated that AuNPs could mimic catalase and superoxide dismutase.[37] On the other hand, AuNPs' plasmonic properties endow them with a remarkable electromagnetic field enhancement, which is able to promote Raman reporters' vibrations placed within the enhanced electromagnetic field.[38] Thus, AuNPs have been successfully employed as SERS-active substrates for developing a number of sensitive chemical and biomedical assays.[1−3,39−42]

The combination of AuNPs' SERS activities and catalytic properties will provide a particularly promising platform for real-time probing of AuNP-catalyzed reactions and for developing sensitive bioassays.[28,43−51] For example, a few recent studies demonstrated the simultaneous use of catalytic and plasmonic properties of AuNPs for monitoring the catalytic reduction of nitrophenol and nitrothiophenol with AuNPs *via* SERS.[52] Although plasmonic nanosensors for DNA detection have been constructed by using AuNPs as oxidase mimics,[43] the combination of AuNPs' enzyme-mimicking properties with their SERS activities for bioassays has yet to be explored. We reason that such a combination would not only lower the bioassays' cost by using cost-effective nanozymes but also provide good sensitivity offered by SERS.

In this work, we prepared AuNPs within MIL-101, a highly porous and thermally stable metal−organic framework (MOF), by an *in situ* reduction strategy (Figure S2). The AuNPs within MIL-101 were denoted as AuNPs@MIL-101. We then demonstrated that AuNPs@MIL-101 acted not only as the peroxidase mimics for catalytically converting Raman-inactive reporters (*i.e.*, caged reporters) into the active ones (*i.e.*, activated reporters) but also as the SERS-active substrates to enhance the active reporters' Raman signals (Scheme 1). Notably, the AuNPs@MIL-101 were further decorated with oxidases to form AuNPs@MIL-101@oxidases integrative nanozymes, which enabled the efficient enzymatic cascade reactions (Scheme 1). The integrative nanozymes were then successfully used to measure the changes of glucose and lactate associated with ischemic stroke in living animal brains. They were also used to evaluate the therapeutic efficacy of potential drugs for alleviating cerebral ischemic injuries. Their general applications were further demonstrated by monitoring glucose and lactate metabolism in tumors.

RESULTS AND DISCUSSION

AuNPs@MIL-101 with Simultaneous Peroxidase-Mimicking and SERS Activities. Although AgNPs may also possess simultaneous enzymatic and SERS properties,[51] they are sensitive to H_2O_2 (Figure S1), which is necessary for the peroxidase-like catalysis. Therefore, AuNPs were chosen in the current study. The synthetic route of the AuNPs@MIL-101-based nanozymes is shown in Figure S2. AuNPs were *in situ* embedded into MIL-101, a model of a nanoscaled MOF host, by a solution impregnation strategy to form the AuNPs@MIL-101 nanozymes.[53] MIL-101, with high porosity and thermal stability, was chosen as the protecting matrix to prevent AuNPs from aggregation especially in complex biological samples.[54,55] The aggregation, if it happened, would severely affect the catalytic activity. The formation of the AuNPs@MIL-101 nanozymes was confirmed by TEM, XRD, and other characterizations,

Scheme 1. Schematic illustration of AuNPs@MIL-101@oxidases for efficient enzymatic cascade reactions. First, oxidases catalyzed the oxidation of a substrate target (*i.e.*, glucose or lactate) to produce H_2O_2; peroxidase-like AuNPs in AuNPs@MIL-101@oxidases then catalytically oxidized caged Raman reporters (*i.e.*, LMG) with H_2O_2 to produce active Raman reporters (*i.e.*, MG) and simultaneously enhanced the reporters' Raman signals for SERS measurements.

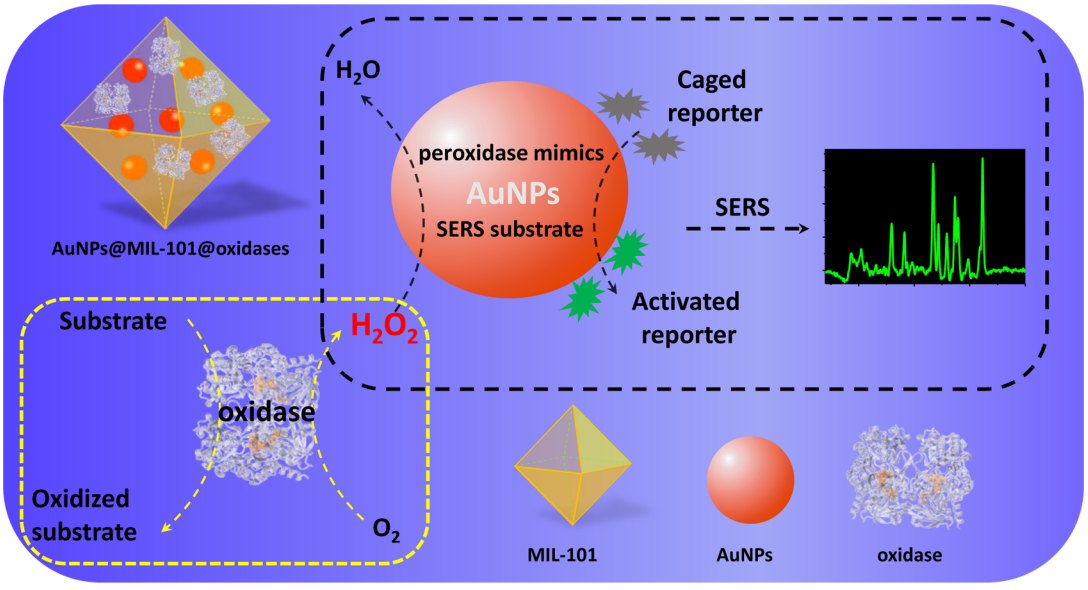

DOI: 10.1021/acsnano.7b00905
ACS Nano 2017, 11, 5558−5566

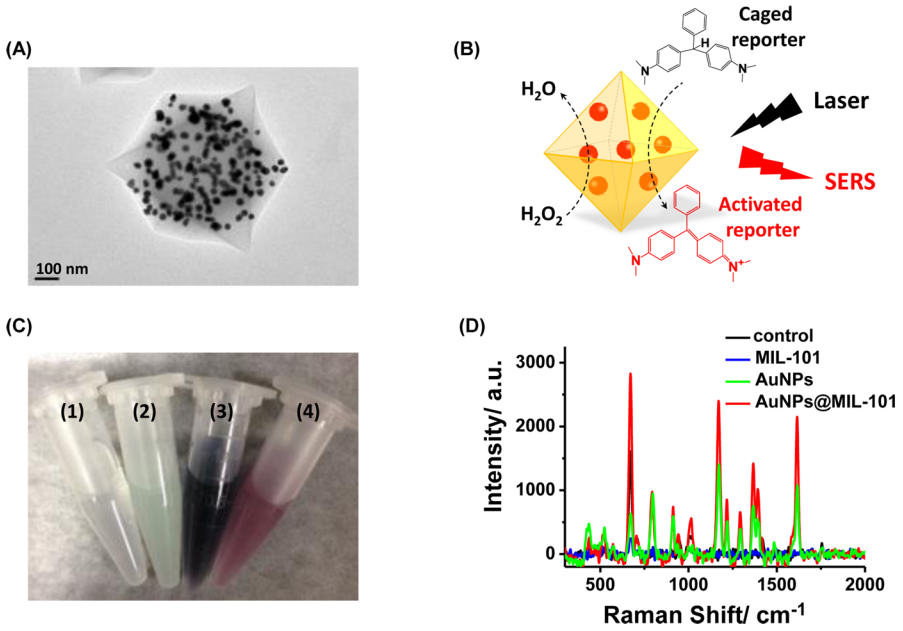

Figure 1. (A) Typical TEM image of AuNPs@MIL-101. (B) Schematic illustration of AuNPs@MIL-101 acting not only as the peroxidase mimics for catalytically converting Raman-inactive reporters leucomalachite green (LMG) into the active ones (malachite green, MG) in the presence of H_2O_2 but also as the SERS substrates for enhancing the active reporters' Raman signals. (C) Photo and (D) corresponding SERS spectra of the samples containing (1) LMG + H_2O_2 (control), (2) LMG + H_2O_2 + MIL-101, (3) LMG + H_2O_2 + AuNPs, and (4) LMG + H_2O_2 + AuNPs@MIL-101 in 50 mM Tris-HCl (pH 7.0).

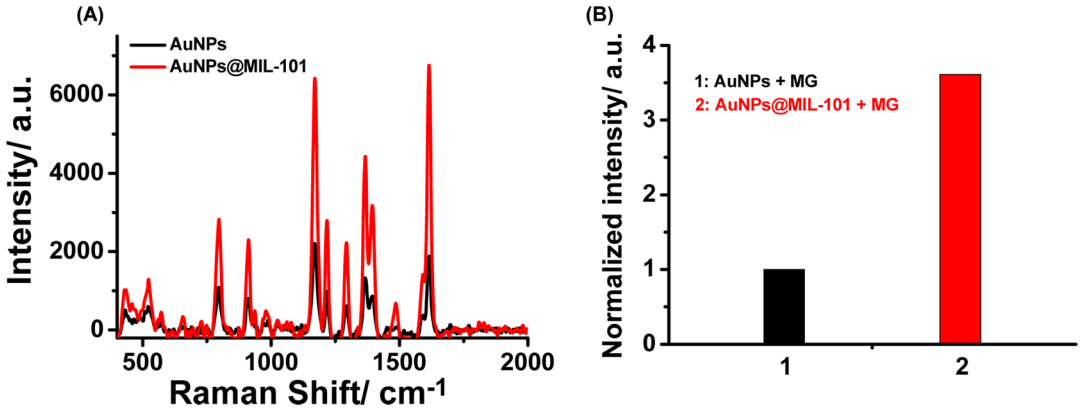

Figure 2. (A) SERS spectra of MG with AuNPs or AuNPs@MIL-101. (B) Normalized SERS signal of MG at 1615 cm^{-1} with AuNPs or AuNPs@MIL-101.

demonstrating the successful incorporation of highly crystalline AuNPs within MIL-101 frameworks (Figures 1A, 3, and S3−S6).

The simultaneous peroxidase-mimicking and SERS activities of the AuNPs@MIL-101 nanozymes were then evaluated (Figure 1B). As shown in Figure 1B and 1D, AuNPs@MIL-101 catalytically oxidized the reduction of caged leucomalachite green (LMG) into malachite green (MG) in the presence of H_2O_2 and produced strong SERS signals, owning to AuNPs' peroxidase-like and SERS activities. In contrast, MIL-101 did not produce any detectable SERS signals, indicating that the biocatalytic and SERS enhancement properties originated from the AuNPs. Although AuNPs themselves could also activate LMG and produce detectable SERS signals (Figure 1D), they were not stable and formed severe aggregation in high-salt solutions (Figure 1C). Such aggregation prevented the use of AuNPs alone for assays in complex biological samples. Moreover, compared with the citrate-protected AuNPs (Figure S1), the AuNPs@MIL-101 exhibited about a 3.6-fold higher SERS response to MG (Figure 2). Therefore, MIL-101 not only provided the AuNPs with much better stability but also exhibited an interesting enrichment effect.[53] These results demonstrated that the AuNPs@MIL-101-based nanozymes possessed both peroxidase-mimicking activity and SERS enhancement property, which could be further explored for activating the reduction of caged Raman reporters for SERS measurements.

It is well known that the enzyme-mimicking and SERS activities are closely related to the size of the AuNPs. Therefore, we synthesized three different sized AuNPs within MIL-101 and investigated their effects on the SERS-active performances, including small size (10 nm) *s*-AuNPs@MIL-101, medium size (38 nm) *m*-AuNPs@MIL-101, and large size (57 nm) *l*-AuNPs@MIL-101. As shown in Figure 3, *m*-AuNPs@MIL-101 exhibited the best SERS-active performance. Therefore, *m*-AuNPs@MIL-101 were used in the subsequent detection.

AuNPs@MIL-101@oxidases for *in Vitro* Detecting Bioactive Small Molecules. AuNPs were reported with both

DOI: 10.1021/acsnano.7b00905
ACS Nano 2017, 11, 5558−5566

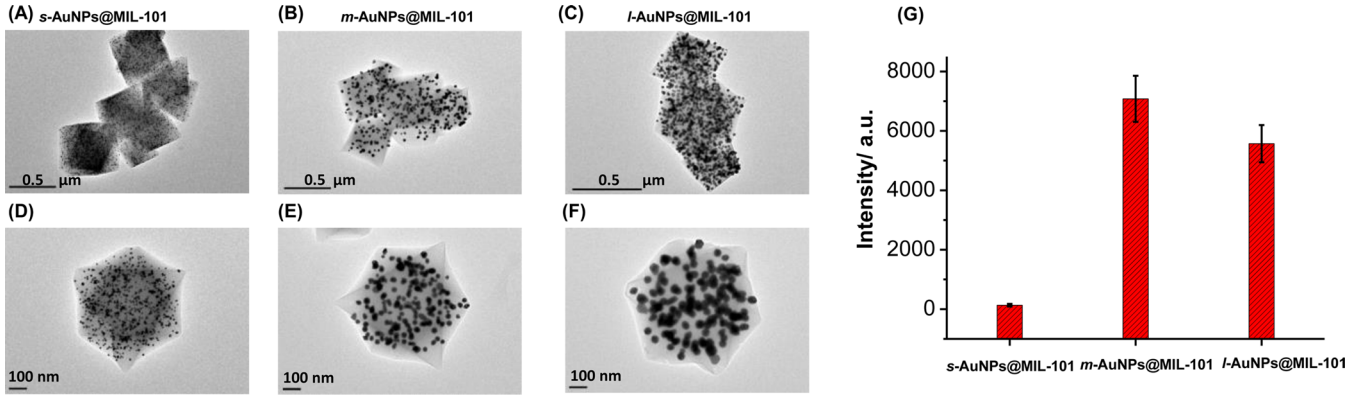

Figure 3. TEM images of *s*-AuNPs@MIL-101 (A and D), *m*-AuNPs@MIL-101 (B and E), and *l*-AuNPs@MIL-101 (C and F). (G) Raman intensity of MG at 1615 cm^{-1} from SERS-active AuNPs@MIL-101 containing different sized AuNPs in 50 mM Tris-HCl buffer (pH = 7.0) with 10 mM H_2O_2 and 1.25 mM LMG. Error bars indicate standard deviations of three independent measurements.

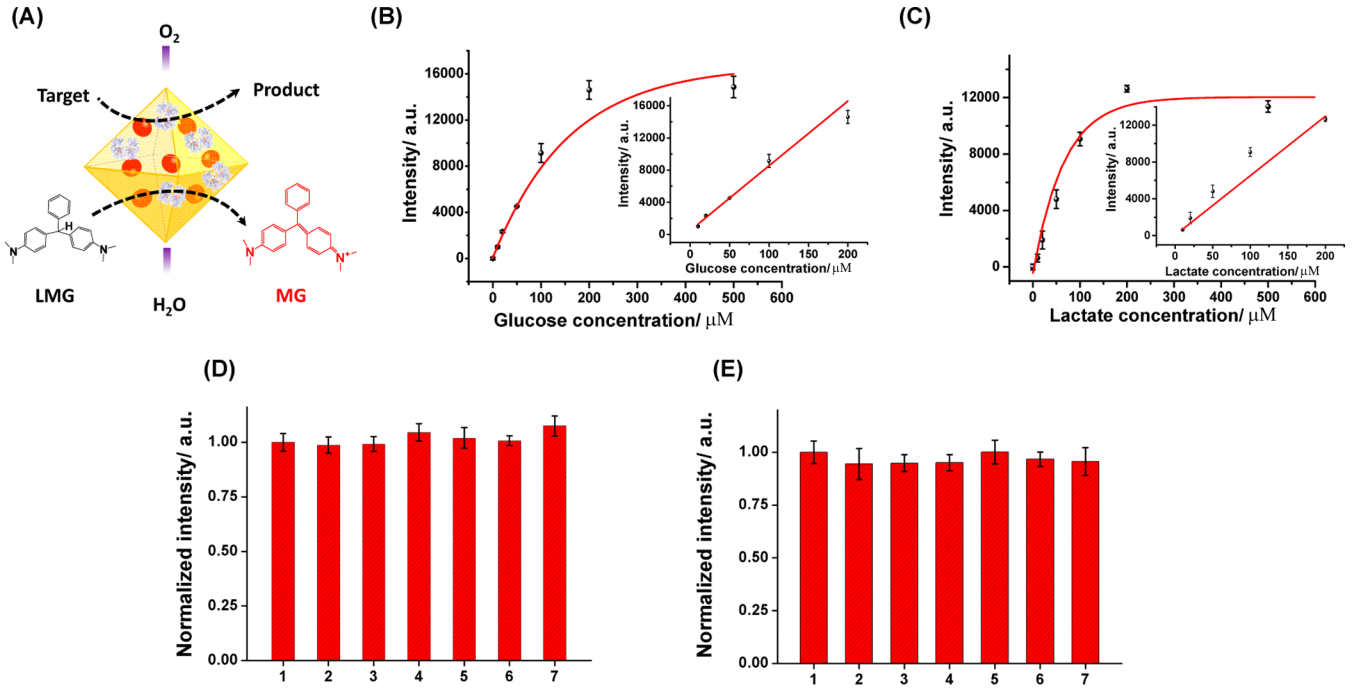

Figure 4. (A) Schematic illustration of *in vitro* detecting glucose (or lactate) with the corresponding integrative nanozymes. (B) Plots of Raman intensity of MG at 1615 cm^{-1} *versus* glucose concentrations. Inset: Linear response to glucose concentrations. (C) Plots of Raman intensity of MG at 1615 cm^{-1} *versus* lactate concentrations. Inset: Linear response to lactate concentrations. (D) Selective detection of 500 μM glucose in the absence (1) and presence of 10 μM 5-HT (2), 10 μM AA (3), 10 μM DA (4), 10 μM DOPAC (5), 1 mM lactate (6), and 10 μM UA (7), respectively. (E) Selective detection of 500 μM lactate in the absence (1) and presence of 10 μM 5-HT (2), 10 μM AA (3), 10 μM DA (4), 10 μM DOPAC (5), 1 mM glucose (6), and 10 μM UA (7), respectively. Final concentrations of AuNPs@MIL-101@oxidases and LMG were 100 μg/mL and 200 μM, respectively. Error bars indicate standard deviations of three independent measurements. Raman intensity of MG at 1615 cm^{-1} for glucose (lactate) was normalized as unity.

GOx-like and peroxidase-like activities, which in principle would enable self-activated cascade catalysis for glucose detection without using GOx.[35] However, *m*-AuNPs@MIL-101 did not show any obvious GOx-mimicking activity (Figure S11). This result demonstrated that it is necessary to couple oxidases for the efficient enzymatic cascade reactions. Previously, we have shown that by coupling two or multiple enzymatic catalysts within a nanoscaled space, the overall efficiency of the enzymatic cascade reactions would be significantly enhanced due to the "nanoscale proximity effects".[56] Therefore, for effectively monitoring bioactive small molecules (*e.g.*, glucose and lactate), integrative nanozymes were constructed. By self-assembling oxidase (*i.e.*, GOx or lactate oxidase, LOx) and AuNPs@MIL-101 together, two integrative nanozymes, AuNPs@MIL-101@GOx and AuNPs@MIL-101@LOx, were obtained (Figure S2).

The cascade catalytic activities of the two integrative nanozymes were first assessed. The assembled oxidase oxidized the substrate (*i.e.*, glucose or lactate) to produce H_2O_2, which would continue to oxidize LMG into Raman-active MG *via* AuNPs' catalysis (Scheme 1). The *in situ* formed MG would then generate SERS signals for measurements (Figure 4A). As shown in Figure S12A, when AuNPs@MIL-101@GOx was added into the solution containing glucose and LMG, the reaction solution produced distinguishable SERS signals after incubation. When MIL-101@GOx was tested, no SERS signals were obtained since MIL-101 was not an effective peroxidase mimic.

DOI: 10.1021/acsnano.7b00905
ACS Nano 2017, 11, 5558−5566

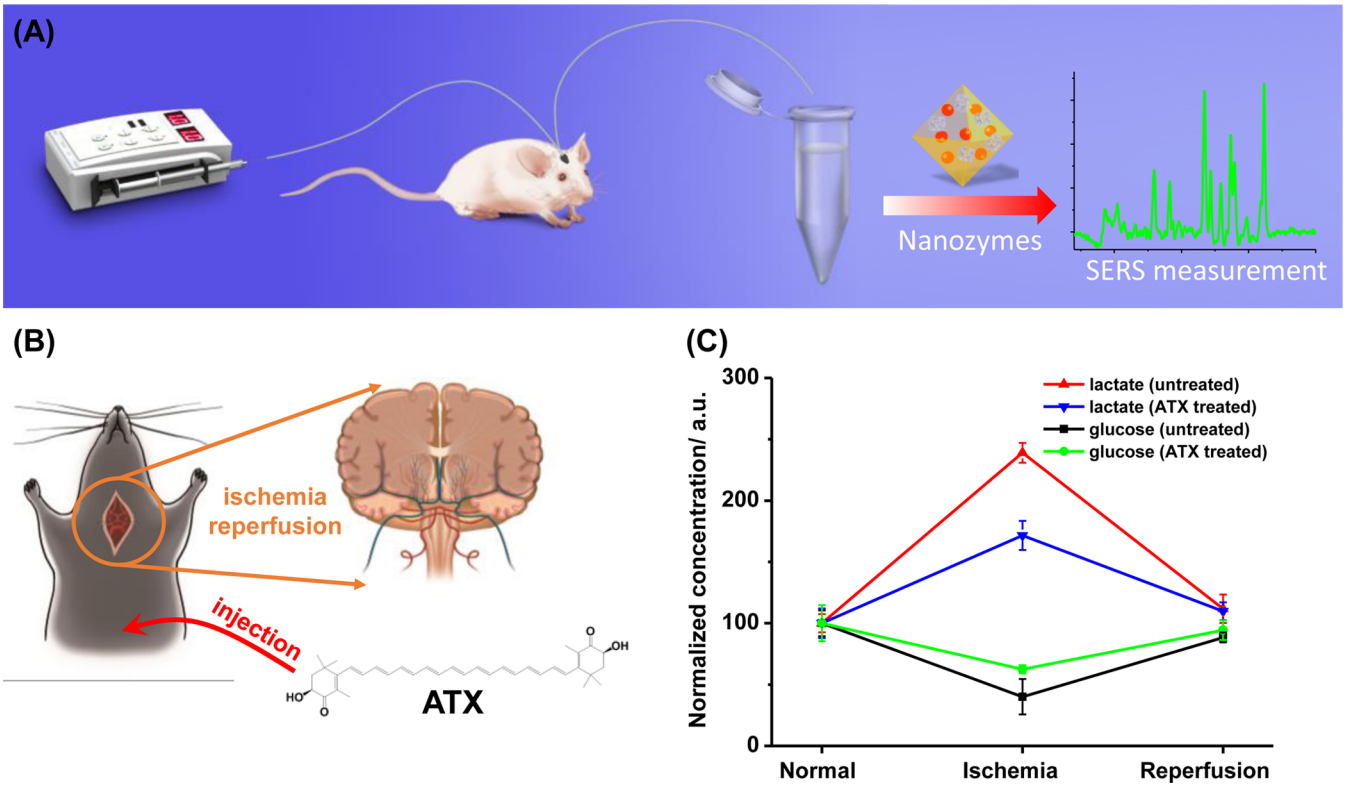

Figure 5. (A) Schematic illustration of monitoring glucose and lactate in living rats' brains with integrative nanozymes based detection platform. (B) Schematic illustration of global cerebral ischemia/reperfusion and the treatment with ATX. Schematic images of mouse and pump were adapted from our previous results.[56] (C) Dynamic changes of glucose and lactate following ischemia and reperfusion with and without ATX pretreatment. The glucose and lactate levels before ischemia were normalized as 100.

Although AuNPs@GOx could also catalyze the cascade reactions to generate detectable SERS signals, they were not very stable, which limited their practical use. For AuNPs@MIL-101@LOx, similar results were observed. These results demonstrated that it would be feasible to detect the bioactive small molecules glucose and lactate by using the corresponding oxidase-containing integrative nanozymes.

We then assessed the *in vitro* sensing performance of the two integrative nanozymes toward glucose and lactate after optimizing the sensing parameters (such as temperature, incubation time, and the loading amounts of oxidases; see Figures S13 and S14). As shown in Figure 4B and C, the SERS signals increased with the increase of glucose (or lactate) concentrations. Moreover, for glucose, a linear range from 10 to 200 μM and a detection limit of 4.2 μM (based on 3δ/s) were obtained, while for lactate, a linear range from 10 to 200 μM and a detection limit of 5.0 μM (based on 3δ/s) were obtained.

Due to the complexity of the biological samples from living brains, it is critical to evaluate the selectivity of the integrative nanozymes based SERS assays. As shown in Figure 4D and E, the key interfering species that coexist with glucose and lactate in living brains were examined, which included sodium ascorbate (AA), dopamine (DA), 3,4- dihydroxyphenylacetic acid (DOPAC), uric acid (UA), and 5- hydroxytryptamine (5-HT). Interestingly, none of them at physiological levels interfered with the glucose and lactate detection.

The results clearly demonstrated the good sensitivity and selectivity of the integrative nanozymes based SERS bioassays for glucose and lactate, which were further explored for monitoring glucose and lactate in living brains.

Monitoring Glucose and Lactate in Living Brains and Evaluating the Therapeutic Efficacy of Astaxanthin (ATX). The above-developed bioassays were further employed to monitor the change of glucose and lactate in living brains following ischemia and reperfusion (Figure 5). Both glucose and lactate are important neurochemicals, which are widely involved in various physiological and pathological brain functions such as ischemia, learning, and memory. As shown in Table 1, after the rats were administrated with global ischemia for 2 h, the striatum glucose level decreased from a basal level of 365.8 ± 38.5 μM (n = 3) (*i.e.*, 100%) to 40.1 ± 14.4% (n = 3). The glucose level then restored to 88.4 ± 4.0% (n = 3) of the basal level during the reperfusion process (Figure 5C and Table 1). On the other hand, the lactate level first increased from a basal level of 573.4 ± 42.6 μM (n = 3) (*i.e.*, 100%) to 239.8 ± 8.1% (n = 3) following ischemia and then restored to 111.8 ± 11.6% (n = 3) during the reperfusion process (Figure 5C and Table 1). The different dynamic response between glucose and lactate during ischemia

Table 1. Glucose and Lactate in the Brain of Living Rats Following Ischemia/Reperfusion without and with ATX Treatment

	glucose/%			lactate/%		
	basal	ischemia	reperfusion	basal	ischemia	reperfusion
without ATX treatment	100	37.4	99.8	100	242.8	134.2
	100	42.5	84.1	100	232.9	98.8
	100	40.2	85.6	100	243.7	104.5
with ATX treatment	100	56.8	78.5	100	195.6	133.3
	100	57.0	98.7	100	156.2	107.0
	100	76.3	109.8	100	166.7	93.5

DOI: 10.1021/acsnano.7b00905
ACS Nano 2017, 11, 5558−5566

could be attributed to the blockage of cerebral blood flow as well as increased anaerobic respiration, *etc.* (Figure S15).[57,58]

Ischemic stroke is one of the leading causes of death in the world. Therefore, it is necessary to develop effective bioassays to evaluate the therapeutic efficacy of potential drugs for preventing ischemic stroke. Here, using ATX as a model antioxidation drug, the above developed assays were employed to evaluate its protective effects against ischemic stroke in living brains.[59] For this purpose, the rats were pretreated with ATX for 1 week before administrating the ischemia, which mimicked ischemic stroke disease (Figure S15). As shown in Figure 5C and Table 1, compared with the control rats without ATX treatment, both the glucose and lactate fluctuation levels were significantly inhibited for the ATX-pretreated rats during ischemia. These results not only demonstrated that ATX could be an effective drug for ischemic stroke but also provided a facile bioassay for evaluation the potential drugs' therapeutic efficacy.

Measuring Glucose and Lactate Metabolism in Normal and Tumor Tissues. To demonstrate the general applications of the integrative nanozymes based SERS bioassays, the glucose and lactate metabolism in normal and tumor tissues was measured. As shown in Table 2, the measured concentrations of glucose and lactate in normal mice tissues were 83.3 ± 4.7 and 16.1 ± 4.1 μM, respectively. Remarkably, the glucose content in tumor tissues was as low as barely measurable. In addition, the lactate content in tumor tissues (187.7 ± 98.7 μM) was more than 10 times higher than that in normal tissues. The difference of glucose and lactate between normal and tumor tissues could be ascribed to the Warburg effect, a metabolic hallmark of tumor cells. Because of the Warburg effect, tumor cells rely on aerobic glycolysis, which is an inefficient way to generate energy. Therefore, tumor cells need to take up and consume more nutrients (*i.e.*, glucose) than normal cells, leading to a much lower glucose level in tumor tissues than in normal tissues. Furthermore, tumor tissues with hypoxia lead to the accumulation of lactate, resulting in a much higher level of lactate in tumor tissues than in normal tissues.[60]

Table 2. Glucose and Lactate in Normal and Tumor Tissues

	glucose/μM	lactate/μM
normal	82	15
	80	12.9
	88	20.5
tumor		192
		89
	4.2	282

CONCLUSIONS

In summary, we have demonstrated the simultaneous peroxidase-mimicking and SERS activities of AuNPs@MIL-101-based nanozymes. AuNPs@MIL-101 can catalytically oxidize caged Raman reporter LMG to Raman-active MG for SERS signaling. The integrative nanozymes were then constructed by assembling oxidases onto AuNPs@MIL-101, which enabled the efficient enzymatic cascade reactions for facile SERS bioassays. *In vitro*, glucose and lactate were successfully detected with good sensitivity and selectivity by using AuNPs@MIL-101@GOx and AuNPs@MIL-101@LOx integrative nanozymes, respectively. Further, the integrative nanozymes were used to monitor the changes of glucose and lactate associated with physiological and pathological conditions (such as ischemic stroke) in living brains and to evaluate the therapeutic effects of ATX for alleviating cerebral ischemic injuries. The developed integrative nanozymes were applicable to investigating other important biological events (such as monitoring glucose and lactate metabolism in tumor tissues). The current work not only demonstrated the great promise of combining AuNPs' multiple functionalities for versatile bioassays but also provided an interesting approach to designing high-performance nanozymes for biomedical applications.

METHODS AND EXPERIMENTAL

Chemicals and Materials. Chromium(III) nitrate ($Cr(NO_3)_3 \cdot 9H_2O$), 1,4-benzene dicarboxylic acid (H_2BDC), hydrofluoric acid, chloroauric acid, sodium citrate dehydrate, leucomalachite green, malachite green, glucose, sodium ascorbate, dopamine, 3,4-dihydroxyphenylacetic acid, uric acid, 5-hydroxytryptamine, L-(+)-lactate acid, glucose oxidase (E.C.1.1.3.4, from *Aspergillus niger*), and astaxanthin (≥97%, from *Haematococcus pluvialis*) were obtained from Sigma and used as received. Lactate oxidase was obtained from TOYBO CO., Ltd. Other chemicals were of at least analytical reagent grade and used as received. The stock solution of LMG was prepared by dissolving LMG into DMSO. Artificial cerebrospinal fluid (aCSF) at pH 7.4 containing NaCl (126 mM), KCl (2.4 mM), KH_2PO_4 (0.5 mM), $MgCl_2$ (0.85 mM), $NaHCO_3$ (27.5 mM), Na_2SO_4 (0.5 mM), and $CaCl_2$ (1.1 mM) was used. Ringer's solution was used as the perfusion solution for *in vivo* microdialysis. The Ringer's solution was prepared by mixing NaCl (147 mM) and $CaCl_2$ (4.4 mM) into deionized water. All aqueous solutions used in the experiments were prepared with deionized water (18.2 MΩ·cm, Millipore).

Instrumentation. Powder X-ray diffraction (XRD) data were collected on an ARL SCINTAG X'TRA diffractometer by using Cu Kα radiation (Thermo). Transmission electron microscopy (TEM) was performed on a JEOL 2100F or FEI TF-20 transmission electron microscope at an acceleration voltage of 200 kV. UV−visible absorption spectra were collected on a UV−visible spectrophotometer with a 1.0 cm quartz cell (Beijing Purkinje General Instrument Co. Ltd., China). Raman spectra were obtained on an Advantage Raman spectrometer (Japan) with a 633 nm laser.

Preparation of MIL-101 and AuNPs@MIL-101. (a) Water-soluble MIL-101 was synthesized as follows.[61,62] A 14.4 mL amount of aqueous solution containing $Cr(NO_3)_3 \cdot 9H_2O$ (1200 mg, 3 mmol), hydrofluoric acid (0.6 mL, 3 mmol), and H_2BDC (492 mg, 3 mmol) was added in a hydrothermal autoclave reactor, which reacted at 220 °C for 8 h. The green product and crystallized H_2BDC byproduct were obtained after natural cooling. The product was purified by washing with DMSO. The purified light green product was dried at 80 °C under vacuum for further experiments. (b) AuNPs@MIL-101 was prepared by a solution impregnation strategy.[53] Briefly, 50 mg of MIL-101 was suspended in 30 mL of 0.1% (w/v) $HAuCl_4$ aqueous solution and was kept under continuous stirring at 45 °C for 2.5 h. Then, the solution was heated to vigorous boiling, followed by quick injection of 220 μL of 30% or 10% (w/v) sodium citrate and further stirring for another 40 min at boiling. After cooling, the AuNPs@MIL-101 products with small-sized and medium-sized AuNPs were collected and purified by centrifugation. The two AuNPs@MIL-101 products were named *s*-AuNPs@MIL-101 and *m*-AuNPs@MIL-101, respectively. The AuNPs@MIL-101 with large-sized AuNPs (called *l*-AuNPs@MIL-101) was obtained by a seed-mediated growth method using *m*-AuNPs@MIL-101 as the seeds. A 2 mL amount of 10 mg/mL seeds was suspended in 12.5 mL of 2.8 mM $NH_2OH \cdot HCl$ aqueous solution and kept under vigorous stirring. Then 150 μL of 50 mM $HAuCl_4$ was added into the above solution, which was further stirred for another 30 min. The *l*-AuNPs@MIL-101 was collected and purified by centrifugation.

Citrate-protected AuNPs were prepared with the same method as AuNPs@MIL-101 without adding MIL-101. Citrate-protected AgNPs were synthesized according to a literature method.[51]

Preparation of AuNPs@MIL-101@oxidases Integrative Nanozymes. A 10 mg sample of AuNP@MIL-101 was redispersed in 900 μL of buffer (50 mM Tris-HCl, pH = 7.0); then 20, 50, 100, or 200 μL of

DOI: 10.1021/acsnano.7b00905
ACS Nano 2017, 11, 5558−5566

10 mg/mL GOx (or LOx) was added to the solution. The resulting mixture was thoroughly mixed and further incubated at 28 °C for 2 h. After centrifugation at 4000 rpm for 5 min to remove the unassembled GOx (or LOx), ~10 mg/mL integrative nanozymes loaded with different amounts of oxidases were obtained.

AuNPs@MIL-101 for Catalytic Oxidation of Caged Raman Reporters and for SERS Measurements. For a typical test, 10 μL of 10 mg/mL AuNPs@MIL-101 was added into 50 mM Tris-HCl buffer (pH = 7.0) containing H_2O_2 (3 μL, 100 mM) and LMG (50 μL, 25 mM). The final volume of the mixed solution was adjusted to 1 mL with the buffer. The mixture was then incubated at 37 °C for 30 min and used for SERS measurements.

***In Vitro* Glucose and Lactate Measurement with AuNPs@MIL-101@oxidases Integrative Nanozymes.** Typically, different concentrations of glucose (or lactate) and AuNPs@MIL-101@GOx (or AuNPs@MIL-101@LOx) were added into 50 mM Tris-HCl buffer (pH = 7.0) containing LMG. The final volume of the reaction solution was adjusted to 1 mL. The final concentration of the integrative nanozymes was 100 μg/mL, and the final concentration of LMG was 200 μM. After incubation for 90 min (at 45 °C for glucose and 37 °C for lactate), the SERS spectra of the reaction solutions were recorded.

Living Brain Ischemia and Reperfusion Surgery. All the animal studies were approved by the Committee for Experimental Animals Welfare and Ethics of Nanjing Drum Tower Hospital, the Affiliated Hospital of Nanjing University Medical School. Male adult Sprague–Dawley rats (250–300 g) were obtained from Jiesijie Laboratory Animal Co. (Shanghai, China). The living brain ischemia and reperfusion surgery of rats was performed following our previous protocols.[56] Briefly, global ischemia (2 h) and reperfusion (2 h) were induced by occluding both carotid arteries with nontraumatic arterial clips for ischemia and then removing the clips for reperfusion. During the surgery, aCSF solution was continuously perfused at 2 μL/min. The samples were collected with a microdialysis probe and diluted by a factor of 10 for further SERS measurements by the integrative nanozyme.

ATX Pretreatment. To study the therapeutic effects of ATX, six rats were randomly divided into two groups. One group (group I) was fed with food and water, while the other group (group II) was not only fed with food and water but also intraperitoneally injected with ATX (10 mg/kg/day) for 7 consecutive days before the ischemia/reperfusion surgery. Four hous before the surgery, group II received ATX (10 mg/kg) treatment once again.

Measuring Glucose and Lactate Metabolism in Normal and Tumor Tissues. Mice bearing xenografted human colon tumors (from CT-26 cells) were chosen as the tumor model. When the tumor sizes were *ca.* 200–250 mm^3, the samples were collected from the tumor using a microdialysis probe. Specifically, a guide needle (0.4 × 40 mm) was intracutaneously inserted into the tumor with a depth of 1–2 mm from the epidermis surface. A linear microdialysis probe (CMA 30) was then carefully inserted through the needle. After carefully removing the needle, the linear microdialysis probe was kept in the tumor for sample collection. The sample collection was performed by perfusing Ringer's solution at 1 μL/min. Before the microdialysis sample collection, the perfusion was run for at least 90 min for equilibration. The samples of normal tissues were collected from the same position of healthy mice under the above referred conditions.

ASSOCIATED CONTENT

Supporting Information

The Supporting Information is available free of charge on the ACS Publications website at DOI: 10.1021/acsnano.7b00905.

Extra figures with associated discussion; tables (PDF)

AUTHOR INFORMATION

Corresponding Authors

*E-mail: zyzhou@nju.edu.cn.

*E-mail: weihui@nju.edu.cn. Web: weilab.nju.edu.cn. Fax: +86-25-83594648. Tel: +86-25-83593272.

ORCID

Shuming Nie: 0000-0002-7328-1144

Hui Wei: 0000-0003-0870-7142

Notes

The authors declare no competing financial interest.

ACKNOWLEDGMENTS

This work was supported by National Natural Science Foundation of China (21405081, 21405079, 21550110189, 81671751, 11474147), Natural Science Foundation of Jiangsu Province (BK20160615, BK20151383), 973 Program (2015CB659400, 2015CB654901), International Science & Technology Cooperation Program of China (2014DFE00200), PAPD program, Shuangchuang Program of Jiangsu Province, Six Talents Summit Program of Jiangsu Province, Open Funds of the State Key Laboratory of Analytical Chemistry for Life Science (SKLACLS1704), Open Funds of the State Key Laboratory of Coordination Chemistry (SKLCC1619), China Postdoctoral Science Foundation (2015M581770, 2016M590437), Social Development Foundation of Jiangsu Province (BE2015605), and Thousand Talents Program for Young Researchers. We thank Prof. Xuejin Zhang for help with Raman measurements and Dr. Meiting Zhao for help with MIL-101 synthesis.

REFERENCES

(1) Anker, J. N.; Hall, W. P.; Lyandres, O.; Shah, N. C.; Zhao, J.; Van Duyne, R. P. Biosensing with Plasmonic Nanosensors. *Nat. Mater.* **2008**, *7*, 442–453.

(2) Xu, L. J.; Lei, Z. C.; Li, J.; Zong, C.; Yang, C. J.; Ren, B. Label-Free Surface-Enhanced Raman Spectroscopy Detection of DNA with Single-Base Sensitivity. *J. Am. Chem. Soc.* **2015**, *137*, 5149–5154.

(3) Kong, K. V.; Lam, Z.; Lau, W. K. O.; Leong, W. K.; Oivo, M. A Transition Metal Carbonyl Probe for Use in a Highly Specific and Sensitive SERS-Based Assay for Glucose. *J. Am. Chem. Soc.* **2013**, *135*, 18028–18031.

(4) Wang, Y.; Zhang, C. H.; Tang, L. J.; Jiang, J. H. Enzymatic Control of Plasmonic Coupling and Surface Enhanced Raman Scattering Transduction for Sensitive Detection of DNA Demethylation. *Anal. Chem.* **2012**, *84*, 8602–8606.

(5) Rosi, N. L.; Giljohann, D. A.; Thaxton, C. S.; Lytton-Jean, A. K. R.; Han, M. S.; Mirkin, C. A. Oligonucleotide-Modified Gold Nanoparticles for Intracellular Gene Regulation. *Science* **2006**, *312*, 1027–1030.

(6) Wittstock, A.; Baeumer, M. Catalysis by Unsupported Skeletal Gold Catalysts. *Acc. Chem. Res.* **2014**, *47*, 731–739.

(7) Stratakis, M.; Garcia, H. Catalysis by Supported Gold Nanoparticles: Beyond Aerobic Oxidative Processes. *Chem. Rev.* **2012**, *112*, 4469–4506.

(8) Vasilikogiannaki, E.; Titilas, I.; Vassilikogiannakis, G.; Stratakis, M. *cis*-Semihydrogenation of Alkynes with Amine Borane Complexes Catalyzed by Gold Nanoparticles under Mild Conditions. *Chem. Commun.* **2015**, *51*, 2384–2387.

(9) Lee, Y.; Angel Garcia, M.; Huls, N. A. F.; Sun, S. Synthetic Tuning of the Catalytic Properties of Au-Fe_3O_4 Nanoparticles. *Angew. Chem., Int. Ed.* **2010**, *49*, 1271–1274.

(10) Liu, D.; Yang, J.; Wang, H. F.; Wang, Z.; Huang, X.; Wang, Z.; Niu, G.; Walker, A. R. H.; Chen, X. Glucose Oxidase-Catalyzed Growth of Gold Nanoparticles Enables Quantitative Detection of Attomolar Cancer Biomarkers. *Anal. Chem.* **2014**, *86*, 5800–5806.

(11) Lopez, N.; Janssens, T. V. W.; Clausen, B. S.; Xu, Y.; Mavrikakis, M.; Bligaard, T.; Norskov, J. K. On the Origin of the Catalytic Activity of Gold Nanoparticles for Low-Temperature CO Oxidation. *J. Catal.* **2004**, *223*, 232–235.

(12) Tsunoyama, H.; Sakurai, H.; Ichikuni, N.; Negishi, Y.; Tsukuda, T. Colloidal Gold Nanoparticles as Catalyst for Carbon-Carbon Bond Formation: Application to Aerobic Homocoupling of Phenylboronic Acid in Water. *Langmuir* **2004**, *20*, 11293–11296.

DOI: 10.1021/acsnano.7b00905
ACS Nano 2017, 11, 5558–5566

(13) Comotti, M.; Della Pina, C.; Matarrese, R.; Rossi, M. The Catalytic Activity of "Naked" Gold Particles. *Angew. Chem., Int. Ed.* **2004**, *43*, 5812−5815.
(14) Wei, H.; Wang, E. Nanomaterials with Enzyme-Like Characteristics (Nanozymes): Next-Generation Artificial Enzymes. *Chem. Soc. Rev.* **2013**, *42*, 6060−6093.
(15) Tonga, G. Y.; Jeong, Y.; Duncan, B.; Mizuhara, T.; Mout, R.; Das, R.; Kim, S. T.; Yeh, Y. C.; Yan, B.; Hou, S.; Rotello, V. M. Supramolecular Regulation of Bioorthogonal Catalysis in Cells Using Nanoparticle-Embedded Transition Metal Catalysts. *Nat. Chem.* **2015**, *7*, 597−603.
(16) Natalio, F.; Andre, R.; Hartog, A. F.; Stoll, B.; Jochum, K. P.; Wever, R.; Tremel, W. Vanadium Pentoxide Nanoparticles Mimic Vanadium Haloperoxidases and Thwart Biofilm Formation. *Nat. Nanotechnol.* **2012**, *7*, 530−535.
(17) Zhang, W.; Hu, S.; Yin, J. J.; He, W.; Lu, W.; Ma, M.; Gu, N.; Zhang, Y. Prussian Blue Nanoparticles as Multienzyme Mimetics and Reactive Oxygen Species Scavengers. *J. Am. Chem. Soc.* **2016**, *138*, 5860−5865.
(18) Xue, T.; Peng, B.; Xue, M.; Zhong, X.; Chiu, C. Y.; Yang, S.; Qu, Y.; Ruan, L.; Jiang, S.; Dubin, S.; Kaner, R. B.; Zink, J. I.; Meyerhoff, M. E.; Duan, X.; Huang, Y. Integration of Molecular and Enzymatic Catalysts on Graphene for Biomimetic Generation of Antithrombotic Species. *Nat. Commun.* **2014**, *5*, 3200−3205.
(19) Vernekar, A. A.; Sinha, D.; Srivastava, S.; Paramasivam, P. U.; D'Silva, P.; Mugesh, G. An Antioxidant Nanozyme that Uncovers the Cytoprotective Potential of Vanadia Nanowires. *Nat. Commun.* **2014**, *5*, 5301−5313.
(20) Xia, X.; Zhang, J.; Lu, N.; Kim, M. J.; Ghale, K.; Xu, Y.; McKenzie, E.; Liu, J.; Yet, H. Pd-Ir Core-Shell Nanocubes: A Type of Highly Efficient and Versatile Peroxidase Mimic. *ACS Nano* **2015**, *9*, 9994−10004.
(21) Shen, X.; Liu, W.; Gao, X.; Lu, Z.; Wu, X.; Gao, X. Mechanisms of Oxidase and Superoxide Dismutation-Like Activities of Gold, Silver, Platinum, and Palladium, and Their Alloys: A General Way to the Activation of Molecular Oxygen. *J. Am. Chem. Soc.* **2015**, *137*, 15882−15891.
(22) Cai, R.; Yang, D.; Peng, S.; Chen, X.; Huang, Y.; Liu, Y.; Hou, W.; Yang, S.; Liu, Z.; Tan, W. Single Nanoparticle to 3D Supercage: Framing for an Artificial Enzyme System. *J. Am. Chem. Soc.* **2015**, *137*, 13957−13963.
(23) Liu, B.; Sun, Z.; Huang, P. J. J.; Liu, J. Hydrogen Peroxide Displacing DNA from Nanoceria: Mechanism and Detection of Glucose in Serum. *J. Am. Chem. Soc.* **2015**, *137*, 1290−1295.
(24) Manea, F.; Houillon, F. B.; Pasquato, L.; Scrimin, P. Nanozymes: Gold-Nanoparticle-Based Transphosphorylation Catalysts. *Angew. Chem., Int. Ed.* **2004**, *43*, 6165−6169.
(25) Fan, K.; Cao, C.; Pan, Y.; Lu, D.; Yang, D.; Feng, J.; Song, L.; Liang, M.; Yan, X. Magnetoferritin Nanoparticles for Targeting and Visualizing Tumour Tissues. *Nat. Nanotechnol.* **2012**, *7*, 459−464.
(26) Gao, L.; Zhuang, J.; Nie, L.; Zhang, J.; Zhang, Y.; Gu, N.; Wang, T.; Feng, J.; Yang, D.; Perrett, S.; Yan, X. Intrinsic Peroxidase-Like Activity of Ferromagnetic Nanoparticles. *Nat. Nanotechnol.* **2007**, *2*, 577−583.
(27) Kim, C. K.; Kim, T.; Choi, I. Y.; Soh, M.; Kim, D.; Kim, Y. J.; Jang, H.; Yang, H. S.; Kim, J. Y.; Park, H. K.; Park, S. P.; Park, S.; Yu, T.; Yoon, B. W.; Lee, S. H.; Hyeon, T. Ceria Nanoparticles that can Protect against Ischemic Stroke. *Angew. Chem., Int. Ed.* **2012**, *51*, 11039−11043.
(28) Luo, W.; Zhu, C.; Su, S.; Li, D.; He, Y.; Huang, Q.; Fan, C. Self-Catalyzed, Self-Limiting Growth of Glucose Oxidase-Mimicking Gold Nanoparticles. *ACS Nano* **2010**, *4*, 7451−7458.
(29) Long, Y. J.; Li, Y. F.; Liu, Y.; Zheng, J. J.; Tang, J.; Huang, C. Z. Visual Observation of the Mercury-Stimulated Peroxidase Mimetic Activity of Gold Nanoparticles. *Chem. Commun.* **2011**, *47*, 11939−11941.
(30) Wang, S.; Chen, W.; Liu, A. L.; Hong, L.; Deng, H. H.; Lin, X. H. Comparison of the Peroxidase-Like Activity of Unmodified, Amino-Modified, and Citrate-Capped Gold Nanoparticles. *ChemPhysChem* **2012**, *13*, 1199−1204.
(31) Lin, Y.; Zhao, A.; Tao, Y.; Ren, J.; Qu, X. Ionic Liquid as an Efficient Modulator on Artificial Enzyme System: Toward the Realization of High-Temperature Catalytic Reactions. *J. Am. Chem. Soc.* **2013**, *135*, 4207−4210.
(32) Zhao, Y.; Huang, Y.; Zhu, H.; Zhu, Q.; Xia, Y. Three-in-One: Sensing, Self-Assembly, and Cascade Catalysis of Cyclodextrin Modified Gold Nanoparticles. *J. Am. Chem. Soc.* **2016**, *138*, 16645−16654.
(33) Lin, Y.; Ren, J.; Qu, X. Nano-Gold as Artificial Enzymes: Hidden Talents. *Adv. Mater.* **2014**, *26*, 4200−4217.
(34) Chen, J. L. Y.; Pezzato, C.; Scrimin, P.; Prins, L. J. Chiral Nanozymes-Gold Nanoparticle-Based Transphosphorylation Catalysts Capable of Enantiomeric Discrimination. *Chem. - Eur. J.* **2016**, *22*, 7028−7032.
(35) Lin, Y.; Li, Z.; Chen, Z.; Ren, J.; Qu, X. Mesoporous Silica-Encapsulated Gold Nanoparticles as Artificial Enzymes for Self-Activated Cascade Catalysis. *Biomaterials* **2013**, *34*, 2600−2610.
(36) Gao, L.; Liu, M.; Ma, G.; Wang, Y.; Zhao, L.; Yuan, Q.; Gao, F.; Liu, R.; Zhai, J.; Chai, Z.; Zhao, Y.; Gao, X. Peptide-Conjugated Gold Nanoprobe: Intrinsic Nanozyme-Linked Immunsorbant Assay of Integrin Expression Level on Cell Membrane. *ACS Nano* **2015**, *9*, 10979−10990.
(37) He, W.; Zhou, Y. T.; Warner, W. G.; Hu, X.; Wu, X.; Zheng, Z.; Boudreau, M. D.; Yin, J. J. Intrinsic Catalytic Activity of Au Nanoparticles with Respect to Hydrogen Peroxide Decomposition and Superoxide Scavenging. *Biomaterials* **2013**, *34*, 765−773.
(38) Stiles, P. L.; Dieringer, J. A.; Shah, N. C.; Van Duyne, R. R. Surface-Enhanced Raman Spectroscopy. *Annu. Rev. Anal. Chem.* **2008**, *1*, 601−626.
(39) Dasary, S. S. R.; Singh, A. K.; Senapati, D.; Yu, H.; Ray, P. C. Gold Nanoparticle Based Label-Free SERS Probe for Ultrasensitive and Selective Detection of Trinitrotoluene. *J. Am. Chem. Soc.* **2009**, *131*, 13806−13812.
(40) Stuart, D. A.; Yonzon, C. R.; Zhang, X. Y.; Lyandres, O.; Shah, N. C.; Glucksberg, M. R.; Walsh, J. T.; Van Duyne, R. P. Glucose Sensing Using Near-Infrared Surface-Enhanced Raman Spectroscopy: Gold Surfaces, 10-Day Stability, and Improved Accuracy. *Anal. Chem.* **2005**, *77*, 4013−4019.
(41) Wang, Y.; Vaidyanathan, R.; Shiddiky, M. J. A.; Trau, M. Enabling Rapid and Specific Surface-Enhanced Raman Scattering Immunoassay Using Nanoscaled Surface Shear Forces. *ACS Nano* **2015**, *9*, 6354−6362.
(42) Lane, L. A.; Qian, X.; Nie, S. SERS Nanoparticles in Medicine: From Label-Free Detection to Spectroscopic Tagging. *Chem. Rev.* **2015**, *115*, 10489−10529.
(43) Zheng, X.; Liu, Q.; Jing, C.; Li, Y.; Li, D.; Luo, W.; Wen, Y.; He, Y.; Huang, Q.; Long, Y. T.; Fan, C. Catalytic Gold Nanoparticles for Nanoplasmonic Detection of DNA Hybridization. *Angew. Chem., Int. Ed.* **2011**, *50*, 11994−11998.
(44) Zong, C.; Chen, C. J.; Zhang, M.; Wu, D. Y.; Ren, B. Transient Electrochemical Surface-Enhanced Raman Spectroscopy: A Millisecond Time-Resolved Study of an Electrochemical Redox Process. *J. Am. Chem. Soc.* **2015**, *137*, 11768−11774.
(45) Wang, C.; Astruc, D. Nanogold Plasmonic Photocatalysis for Organic Synthesis and Clean Energy Conversion. *Chem. Soc. Rev.* **2014**, *43*, 7188−7216.
(46) Larsson, E. M.; Langhammer, C.; Zoric, I.; Kasemo, B. Nanoplasmonic Probes of Catalytic Reactions. *Science* **2009**, *326*, 1091−1094.
(47) Zhong, J. H.; Jin, X.; Meng, L.; Wang, X.; Su, H. S.; Yang, Z. L.; Williams, C. T.; Ren, B. Probing the Electronic and Catalytic Properties of a Bimetallic Surface with 3 nm Resolution. *Nat. Nanotechnol.* **2017**, *12*, 132−136.
(48) Novo, C.; Funston, A. M.; Mulvaney, P. Direct Observation of Chemical Reactions on Single Gold Nanocrystals Using Surface Plasmon Spectroscopy. *Nat. Nanotechnol.* **2008**, *3*, 598−602.
(49) Jiang, Z.; Gao, P.; Yang, L.; Huang, C.; Li, Y. Facile *in Situ* Synthesis of Silver Nanoparticles on the Surface of Metal-Organic Framework for Ultrasensitive Surface-Enhanced Raman Scattering Detection of Dopamine. *Anal. Chem.* **2015**, *87*, 12177−12182.

DOI: 10.1021/acsnano.7b00905
ACS Nano 2017, 11, 5558−5566

(50) Cai, Q.; Lu, S.; Liao, F.; Li, Y.; Ma, S.; Shao, M. Catalytic Degradation of Dye Molecules and *in Situ* SERS Monitoring by Peroxidase-Like Au/CuS Composite. *Nanoscale* **2014**, *6*, 8117−8123.
(51) McKeating, K. S.; Sloan-Dennison, S.; Graham, D.; Faulds, K. An Investigation into the Simultaneous Enzymatic and SERRS Properties of Silver Nanoparticles. *Analyst* **2013**, *138*, 6347−6353.
(52) Joseph, V.; Engelbrekt, C.; Zhang, J.; Gernert, U.; Ulstrup, J.; Kneipp, J. Characterizing the Kinetics of Nanoparticle-Catalyzed Reactions by Surface-Enhanced Raman Scattering. *Angew. Chem., Int. Ed.* **2012**, *51*, 7592−7596.
(53) Hu, Y.; Liao, J.; Wang, D.; Li, G. Fabrication of Gold Nanoparticle-Embedded Metal-Organic Framework for Highly Sensitive Surface-Enhanced Raman Scattering Detection. *Anal. Chem.* **2014**, *86*, 3955−3963.
(54) Sugikawa, K.; Nagata, S.; Furukawa, Y.; Kokado, K.; Sada, K. Stable and Functional Gold Nanorod Composites with a Metal-Organic Framework Crystalline Shell. *Chem. Mater.* **2013**, *25*, 2565−2570.
(55) Moon, H. R.; Lim, D.-W.; Suh, M. P. Fabrication of Metal Nanoparticles in Metal-Organic Frameworks. *Chem. Soc. Rev.* **2013**, *42*, 1807−1824.
(56) Cheng, H.; Zhang, L.; He, J.; Guo, W.; Zhou, Z.; Zhang, X.; Nie, S.; Wei, H. Integrated Nanozymes with Nanoscale Proximity for *in Vivo* Neurochemical Monitoring in Living Brains. *Anal. Chem.* **2016**, *88*, 5489−5497.
(57) Zhang, M.; Yu, P.; Mao, L. Rational Design of Surface/Interface Chemistry for Quantitative *in Vivo* Monitoring of Brain Chemistry. *Acc. Chem. Res.* **2012**, *45*, 533−543.
(58) Lin, Y.; Yu, P.; Hao, J.; Wang, Y.; Ohsaka, T.; Mao, L. Continuous and Simultaneous Electrochemical Measurements of Glucose, Lactate, and Ascorbate in Rat Brain Following Brain Ischemia. *Anal. Chem.* **2014**, *86*, 3895−3901.
(59) Naguib, Y. M. A. Antioxidant Activities of Astaxanthin and Related Carotenoids. *J. Agric. Food Chem.* **2000**, *48*, 1150−1154.
(60) Vander Heiden, M. G.; Cantley, L. C.; Thompson, C. B. Understanding the Warburg Effect: The Metabolic Requirements of Cell Proliferation. *Science* **2009**, *324*, 1029−33.
(61) Ferey, G.; Mellot-Draznieks, C.; Serre, C.; Millange, F.; Dutour, J.; Surble, S.; Margiolaki, I. A Chromium Terephthalate-Based Solid with Unusually Large Pore Volumes and Surface Area. *Science* **2005**, *309*, 2040−2042.
(62) Zhao, M.; Yuan, K.; Wang, Y.; Li, G.; Guo, J.; Gu, L.; Hu, W.; Zhao, H.; Tang, Z. Metal-Organic Frameworks as Selectivity Regulators for Hydrogenation Reactions. *Nature* **2016**, *539*, 76−80.

DOI: 10.1021/acsnano.7b00905
ACS Nano 2017, 11, 5558−5566